Near-frequency photons Y-splitter

Near-Frequency Photons Y-Splitter

Riccardo Castagna,[a,] Daniele E. Lucchetta,[b] Massimo Rippa,[a] Ji-Hua Xu,[c] Andrea Di Donato[d]*

[a] *Istituto di Scienze Applicate e Sistemi Intelligenti "E. Caianiello", Via Campi Flegrei, 34, 80078 Pozzuoli (Napoli), Italia*
[b] *Dipartimento di Scienze e Ingegneria della Materia, dell'Ambiente ed Urbanistica, SIMAU, Università Politecnica delle Marche, Via Brecce Bianche, 60131 Ancona, Italia.*
[c]*NEST, Scuola Normale Superiore, Complesso San Silvestro, P.zza San Silvestro, 12, 56127 Pisa, Italia.*
[d]*Dipartimento di Ingegneria dell'Informazione, DII, Università Politecnica delle Marche, Via Brecce Bianche, 60131 Ancona, Italia.*

Keywords: photo-polymerization holography, light matter interaction, Moirè, structured-light, structured matter

ABSTRACT

We are reporting on a wavelength-controlled anomalous angular light scattering with a very high spatial angular dispersion in correspondence to a very small frequencies range. Essentially, we present a device able to Y-split in-air wavelengths of a laser beam few tens of nanometers away from each other. We explain its working mechanism through Moirè-interactions between structured-light and all-dielectric matter structured by light. More precisely, we ascribe this effect to Moiré-beats between holographic patterns recorded in a material and a spatially modulated wave-front of a probe-beam with slightly different spatial frequency content.

INTRODUCTION

Diffractive Optical Elements (DOEs) [1] are usually exploited to get structured-light. The behavior of a light scattered from a DOE depends on its incidence angle, wavelength and, obviously, on the physical and geometrical characteristics of the DOE. As an example, computer-controlled DOEs, usually based on addressable Liquid Crystal (LC) matrices, allow wavefront changes of laser beams and represent the basic working elements of Spatial Light Modulators (SLMs) [2]. A kind of interaction between light "shaped" by two identical superimposed DOEs is the well-known Moirè-effect. This effect was widely investigated in the past especially in relationship to the essential features of **Moiré patterns**, such as their orientation and period [3-8], e.g. Moirè-effect has been used for tunable varifocal Fresnel

lenses [6]. Recently, we have introduced the possibility of generating beats by the interaction between a light-pattern and a previously patterned polymer [9]. Here, we demonstrate - experimentally and theoretically – an anomalous angular light scattering (similarly to meta-materials [10]). It is achieved by the joined effect of a holographic writing process and a successive reading process involving a spatially modulated wave-front of a probe-beam. We explain these effects by considering Moiré-beats between a pattern "recorded in" the material (as a modulation of the real part of the refractive index) and the structured probe-light "impinging on" the material with a slightly different spatial frequency. There is no evidence reported in literature about the use of Moirè-interactions to achieve anomalous **redirection of light**. In particular, in the following we report on the dependence of the diffracted light angle on the difference $\Delta\lambda$ between a polymerizing wavelength λ_w (lambda-writing) and a probe-one λ_r (lambda-reading). In other words, the system we propose distinguishes between $\Delta\lambda > 0$ and $\Delta\lambda < 0$ by redirecting the scattered light in two opposite directions, that is the focus of our manuscript, namely a wavelength-dependent photons Y-splitter. As a relevant consequence of this behavior, it is possible to store and retrieve wavelength and angle of incidence of a polymerizing laser-light and to retrieve the wavelength and the angle of incidence of an incoming light-probe, by just observing the optical far field pattern of the scattered probe light. The consequences of such interaction are of potential interest for a wide spectrum of applications related to different areas of science and technology, such as **Optical Data Storage** (**ODS**) [11], structured-light microscopy, **that is known to be based on Moirè interactions, [12-14]** all optical control over the light directionality,[15-18] discrete achromatic optical elements technology (light-weight collimators, chromatically corrected imaging systems), micro-lenses, [1] branch-Y-optical frequencies spectral switchers [19] wavelength selective couplers and splitters. [20]

EXPERIMENTAL RESULTS

Our system is made by a photo-polymerizable film (thickness ~ 5 μm; see Experimental Section for further details) spin coated on a glass substrate. A single unfocused beam laser $\lambda_w = 514.5\,nm$ is used (without further optical elements**), at the first step,** to induce photo-polymerization of the thin film. In the second step, a **different wavelength** probe beam, such as $\lambda_r = 632.8\,nm$, is used to observe the light transmitted through the polymerized sample. In this condition, concentric rings are projected on a screen placed at the back of the sample: the picture in Figure 1a illustrates this (see also Movie MS1 regarding the concentric rings formation). By slightly rotating the sample (Figures 1b-f) the system gives rise to a visible shift of the center of the concentric rings along the direction of the sample rotation. **This phenomenon regards $\Delta\lambda = \lambda_r - \lambda_w < 0$, whereas** for $\Delta\lambda > 0$, the shift of the center of the concentric rings is opposite with respect to the sample's rotation (Figure 2). The angular distribution of the scattered light (θs) is dependent on both $\Delta\lambda$ magnitude and sign, as shown in the graph of Figure 2. In particular, we report on the angular distribution of the scattered light by fixing the incident angle of the probes $\theta ir = 0.18°$, while the writing angle θiw has a normal incidence. This is a particular case of $\theta ir \neq \theta iw$. Two series of measurements are reported: a) $\lambda w = 514.5\,nm$, while the probes are $\lambda r = 501.5\,nm$ ($\Delta\lambda = 13\,nm$), $496.5\,nm$ ($\Delta\lambda = 18\,nm$), $488\,nm$ ($\Delta\lambda = 26.5\,nm$), $476.5\,nm$ ($\Delta\lambda = 38\,nm$), $472.5\,nm$ ($\Delta\lambda = 42\,nm$) , $457.9\,nm$ ($\Delta\lambda = 56.6\,nm$); (b) $\lambda w = 457.9\,nm$, while the probes are $\lambda r = 472.5\,nm$ ($\Delta\lambda = -14.6\,nm$), $476.5\,nm$ ($\Delta\lambda = -18.6\,nm$), $488\,nm$ ($\Delta\lambda = -30.1\,nm$), $496.5\,nm$ ($\Delta\lambda = -38.6\,nm$), $501.5\,nm$ ($\Delta\lambda = -43.6\,nm$), $514.5\,nm$ ($\Delta\lambda = -56.6\,nm$). At this stage, by considering RSG (Rings-Sample Gap) as the distance (in cm) between the sample and the point where the concentric rings start to be visible, we assume RSG as an indirect evaluation of the distance of the sample from the focal point of an eventual lens represented by the sample. Figure 3 shows the distance RSG vs $\Delta\lambda$.

The result is that RSG depends on the magnitude of $\Delta\lambda$ and on its sign. Furthermore, for low $\Delta\lambda$ there are at least two different λ focusing at the same focus (each one regarding $\Delta\lambda$ having similar magnitude and different sign). Moreover, for higher positive $\Delta\lambda$ a plateau behavior seems to be achieved.

THEORY

The mechanism at the basis of the phenomenon can be separated into three main parts: a) **a well-defined light-intensity distribution (concentric rings pattern) is generated due to the interference of scattered coherent light by the glass slide (1 mm thickness ITO-glass; we have used ITO to increase the reflectivity and surface roughness of the glass cavity)**; **b) this spatial distribution is recorded in a permanent manner as refractive index modulation by photo-polymerization of a thin polymeric film deposited on the glass [9];** c) **spatial Moiré-beats are generated by mutual interactions between the light intensity distribution of the probe beam and the recorded refractive index modulation producing, as a consequence, the characteristic optical far-field patterns** (Figures S1A, S1B, and Movie MS1). **The phenomenon can be explained** by considering the generation of an interference pattern of light - having writing wavelength λ_w - recorded in the polymeric material connected to it (sketch in Figure S1b). The interaction between the recorded pattern and the new one generated by the reading wavelength λ_r $(\neq \lambda_w)$ gives rise to a Moirè-effect. This is mathematically described by a convolution product between the spatial frequency distribution of refractive index recorded in the polymer and spatial frequency distribution of the incoming optical field (see also Supporting information, Figures S2-S7).† In detail, the relation regarding the scattered field distribution is summarized by the following equation (see also **Ref. [9, 21 - 23]):**

(1) $$a_s(k_{rs}) \cong -\frac{j}{2}\int_{-\infty}^{+\infty} \widetilde{e_i}(k_{ri}) c_{is}^0 \widetilde{\Delta\varepsilon}(k_{rs} - k_{ri}) dk_{ri} = -\frac{j}{2}\, c_{is}^0 \widetilde{e_i} * \widetilde{\Delta\varepsilon}$$

in which $a(\kappa_{rs})$ is the complex amplitude of the scattered field, obtained as a convolution in the frequency domain between the spatial Fourier transforms of the incident field $e_i(k_{ri})$ and the dielectric perturbation $\Delta\varepsilon(\kappa_{ri})$ induced by light in the material, having assumed a large pattern distribution compared to the incident wavelength. The convolution is weighted by a coupling coefficient c^0_{is}, describing the amount of interaction between the optical and refractive index distributions. According to its property of translation invariance, the convolution function allows for the description of the spatial frequency modulation induced on the scattered field by the refractive index distribution $\Delta\varepsilon(k_{ri})$. The equation 1 is derived by the description of the interaction between each incident spatial frequency, forming the spatial spectrum of the incident optical pattern, and the continuum spectrum of diffracted waves at the interface polymer-air. The distributions $\tilde{e}_i(k_{ri})$ and $\Delta\tilde{\varepsilon}(k_{ri})$ are complex functions defined in the spatial frequency domain and bring with them all the information about the phase and amplitude changes occurring in the scattered wave. Equation 1 includes the Generalization of Snell's law (GSL) [1] when taking into account that the numerical simulations report on the interface between polymer and glass. In fact, the thin polymeric film, in which the Moirè-pattern is recorded, could introduce an abrupt phase shift (phase discontinuity) at the interface between polymer and glass. This discontinuity is then interacting not just with a single plane wave (as described by GSL), but with a more complex incident field pattern (diffraction figures) generated by small particles on the ITO-coated glass (the theoretical description is reported in Supplementary Information). The result of the convolution product is a pattern having spatial frequency *(sf)* dependent on $\Delta\lambda$ (being $\Delta\lambda = \lambda w - \lambda r$) (Figure S1). In particular, *sf* increases when increasing the magnitude of $\Delta\lambda$. The

theoretical curves for the reported phenomenon are described as dashed red lines in **Figure S2**.

DISCUSSION

When many wavelengths and $\Delta\lambda$ (> 0 and < 0) are analyzed there is evidence of curves related to $\Delta\lambda > 0$ and $\Delta\lambda < 0$ that are similar but not identical. In other words, the system is not perfectly symmetrical. In particular, there are differences in the behavior (slope) of the decay/growth if $\Delta\lambda$ is positive (Figure S2A) or negative (Figure S2B). This observation, in apparent contrast with the analytical description adopted, is explainable when considering the photo-initiator used (CQ, see Supporting information) is more efficient in regions of its maximum absorbance (~ 470 nm). This should cause different polymerization degrees and, as a consequence, different refractive index distributions depending on the writing wavelengths used. However, the system shows more remarkable differences between positive and negative $\Delta\lambda$ concerning the angular deflection of the scattered light. In particular, we checked the direction of the scattered light for positive or negative $\Delta\lambda$ to find a correlation between the orientation of the diffraction angle and the sign of $\Delta\lambda$. Thus, an initial empirical approach is simply based on the measurement of the angular response of the scattered light when rotating the sample; namely, when the incident angle θir of the probe-light is different from θiw that is the writing one. As is visible in Figure 1, a slight rotation of the sample with a pattern written at $\lambda w = 514.5\, nm$ gives rise to a visible shift of the center of the concentric rings along the direction of the sample rotation, when the reading probe is $\lambda r = 632.8\, nm$ (in a first approximation, the correlation between the angle of rotation $\Delta\theta$ and the shift of the concentric rings θs is linear as shown in the graph reported in **Figure S3** of Supp. Info). Furthermore, and surprisingly, for a fixed θir different from θiw, the aforementioned shift is positive or negative depending on the sign of $\Delta\lambda$ (see Figure 2 and compare **Movies MS2** and

MS3). In synthesis, a) if $\Delta\lambda < 0$, then $\theta s > 0$ (positive shift); b) if $\Delta\lambda > 0$, then $\theta s < 0$ (negative shift), as shown in Figure 2. Such a behavior cannot be explained just as a diffraction of a plane wave by a DOE, but it must be described by considering the diffraction between a structured pattern of light and a DOE. In order to explain it, we again theoretically refer to the model retrieved by the Equation 1 describing Moirè-interactions by means of Couple Mode Theory (CMT) [21,22]. According to that, the generation of the anomalous light-scattering distribution is related to the interaction (beating/diffraction) between the incident optical intensity distribution of light and the refractive index distribution of the polymeric thin film. The refractive index of the multi-acrylate monomer before polymerization is around 1.49, while after polymerization we assume ~ 1.51. The final refractive index pattern $\Delta\varepsilon(\boldsymbol{r})$, interacts with the reading pattern of light (shaped by the same optical cavity) and gives rise to the Moiré effect. According to the eq. (1), the amount of refractive index change affects mainly the contrast of the final recorded interference pattern, while the spatial pattern distribution in the recording plane is determined by the spatial frequencies of the two interacting patterns. At this stage, a geometrical approach makes it possible to distinguish between positive and negative $\Delta\lambda$ (**Scheme S1a and b,** in Supporting information). In fact, when tilting the sample, the center of the pattern recorded in the polymer is shifted with respect to the center of the new pattern of light generated by the incoming slightly tilted beam and exiting from the resonance cavity. Therefore, simulations are performed by considering two concentric ring patterns slightly shifted with respect to each other that are superimposed throughout the convolution product: a good correlation between the numerical simulation for the near field pattern and the results is found: Figure 2 indicates the theoretical curve (line) and experimental data (squares; see also the graphs in **Figure S4** to visualize the analogy between experimental and theory; while for the visualization of the effect we direct you to MS2 and MS3). A comparative analysis of Figures 1 and 2 shows that the deflection of the scattered light is dependent: a) on the angle of incidence of the light-

probe with respect to the writing one, b) on the magnitude of $\Delta\lambda$ and c) on its sign. The first of these three observations indicate a correlation with the lens effect. In particular, by fixing the angle of incidence of the incoming light-probe different from the writing one,[λ] the deflection angle of the scattered light decreases by increasing the magnitude of $\Delta\lambda$. On this basis, it is to be expected that the scattered light should converge to different focuses dependent up on different $\Delta\lambda$. Furthermore, on the basis of the observation c) the same magnification should be obtainable by different $\Delta\lambda$ and, as consequence, by different wavelengths. Thus, we assume as an indirect measurement of the focal length the distance from the sample at which the rings first appear visible and measurable. **Figure 3** reports on the focus of a lens effect (see also Supporting Information, **Scheme S2**). In particular, it is evident that the focal length seems dependent on the magnitude of Δλ. Convergence in our system is possible due to the optical path of deflection of the incoming light. Thus, when an intensity distribution of light having a certain frequency impinges on the patterned material having close and lower frequency ($\Delta\lambda < 0$), the final result is a convergent lens. $\Delta\lambda > 0$ brings also to a lens having the focal length shorter than the previous one. To summarize, for short Δλ, the system is able to focus only two wavelengths on the same point (Figure 3, Scheme S2); whereas, considering higher Δλ values the focal lengths approaches the same value for higher positive Δλ, as shown in the graph of Figure 3 and also deducible from the graph of Figure 2. This system can eventually be transformed in a multi-wavelength lens. Numerical simulations (graphs of **Figure S5**) are reported taking into account a relatively thick film (20 μm) for $\Delta\lambda > 0$ and for $\Delta\lambda < 0$. In both the cases, a focus effect is evident (a self-focusing effect for Δλ = 0 is observed when the light-sensitized monomer is contained and irradiated in a glass cuvette ~ 10 mm long and large ~ 0.5 mm (**Figure S6**)). The combination of this behavior and the ability of the system to record information, allows the ability to write multiple times in the material, permitting the multiplexing of the information. Thus, at this stage, we briefly account (**Figure S7**) on the superimposition of patterns visible by using reading-light (probe, $\lambda_r = 632.8\,nm$) and

recorded, in sequence, by the use of three different wavelengths ($\lambda_w = 514.5\,nm;\ 496.5\,nm;\ 488\,nm$) impinging on the same spot, each time at a different angle of incidence of incoming light. The final image is an interferogram obtained as a superimposition of all the wavelengths recorded at many different angles, **from which by image subtraction or back rotation (de-multiplexing), is possible to retrieve all the information recorded in the system**.

CONCLUSIONS

In conclusion, we report on a wavelength-controlled anomalous angular light scattering that is dependent on the difference between the wavelengths of a polymerizing and probing laser incident on a photo-polymerizable film deposited on a glass. This behavior is the join effect, achieved by combining a holographic writing process inside a polymer thin film and a successive reading process by a modulated wave-front of light, involving the Moiré effect. Moiré-interactions between structured-light and matter-structured-by-light are experimentally and mathematically described. The observed effect can be developed in future applications for designing compact lenses having convergent behavior and focus. Furthermore, the proposed system is an optical memory for high density data storage due to its high spectral angular resolution.

Experimental

Materials: di-pentaerythritol-hydroxy-penta/hexa-acrylate (DPEPA) and (1R,4S)-1,7,7,tri-methyl-bi-cyclo[2.2.1]heptane-2,3-dione (Camphorequinone, CQ) are purchased from Sigma-Aldrich and used without further purifications.

Methods:

- Mixture preparation. The solution used for the experiments is made by 6 % (w/w) of (1R,4S)-1,7,7-trimethylbicyclo[2.2.1]heptane-2,3-dione in DPEPA (1 gr of the solution is

prepared in a 5 ml small bottle). The mixture is kept in the dark, at room temperature under magnetic stirring for one week before being used in the experiments.

- **Polymer film preparation**. It is achieved in 2 steps: a) a micro-droplet of the pre-polymerized mixture is used to "wash" the sample. Then b) ~ 5 µm thick film is placed on an ITO-glass slide by spin coating on the slide side opposite to that of the ITO layer. The 15-30 nm thick ITO layer is used to enhance the reflectivity and the roughness of the glass.

- Optical set-up. The sample is placed on a motorized Micrometric Goniometer controlled by a computer. Forward scattering is observed on a black screen placed at 20.8 cm behind the sample. Measurements were carried out by using a laser source Argon Laser (Coherent) with different available wavelengths (454.5 nm; 457.9 nm; 472.5 nm; 476.5 nm; 488 nm; 496.5 nm; 501.5 nm; 514.5 nm), and an He-Ne laser source at λ = 632.8 nm.

The power for the writing procedure is set at P = 78 mW, the one for the reading is set at P = 10 mW.

The correspondent energy densities are $\varepsilon_w = 0.37\, J/\mathrm{mm}^2$ for recording (writing) and $\varepsilon_r = 0.012\ J/mm^2$ for reading, in order to avoid any additional recording effects.

The light scattered by the sample is recorded by using a digital camera SONY, super steady shot, DSC-W90, 8.1 M Pixels, equipped with Carl Zeiss objective, Vario-Tessar, 2.8 - 5.2 / 5.8 - 17.4.

- Software. The images are processed by using *ImageJ* software. The numerical analysis and model are respectively developed and implemented by means of a developed home-made Matlab code.

(ג) We chosen the normal incidence for the writing wavelength and $\theta ir = 0.18°$ for a better readability.

.

References

[1] Aieta, F., Kats, M. A., Genevet, P., Capasso, F., Multiwavelength achromatic metasurfaces by dispersive phase compensation , *Science* **347**, 1342-1345 (2015).

[2] Litchinitser, N. M. Structured Light Meets Structured Matter, *Science*, **337**, 1054-1055, (2012).

[3] Post, D., Han, B., Ifju, P., High Sensitivity Moiré: Experimental Analysis for Mechanics and Materials 1994, Springer Ed.**;** De Angelis, M., De Nicola, S., Ferraro, P., Finizio, A., Pierattini, G. Analysis of Moire fringes for measuring the focal length of lenses, *Optics and Lasers in Engineering*, **30**, 279-286 (1998).

[4] Stefan Bernet, Monika Ritsch-Marte, "Adjustable refractive power from diffractive moiré elements, 2008, Applied Optics, 47, 21, 3722-3730.

[5] Stefan Bernet, Walter Harm, Monika Ritsch-Marte, Demonstration of focus-tunable diffractive Moiré-lenses, Optics Express, 2013, 21, 6, 6955.

[6] Zhaowei Liu, Stéphane Durant, Hyesog Lee, Yuri Pikus, Yi Xiong, Cheng Sun, Xiang Zhang, Experimental studies of far-field superlens for sub-diffractional optical imaging, 2007, 15, 11 Optics Express, 6946.

[7] A. W. Lohmann, A New Class of Varifocal Lenses, Applied Optics, 1970, 9, 7, 1669.

[8] A. W. Lohmann and D. P. Paris, Appl. Opt. 6, 1567 (1967).

[9] R Castagna, A Di Donato, L Nucara, JH Xu, DE Lucchetta, F Simoni, Optics Letters, 2016, 41, 7, 1462-1465.

[10] Metamorphose VI AISBL, The Virtual Institute for Artificial Electromagnetic Materials and Metamaterials, http://www.metamorphose-vi.org/index.php/metamaterials.

[11] Castagna, R. , Vita, F., Lucchetta, D. E., Criante, L., Simoni, F., Superior-Performance Polymeric Composite Materials for High-Density Optical Data Storage, 21, 589–59 (2009);

[12] Bailey B, Farkas DL, Taylor DL, Lanni F "Enhancement of axial resolution in fluorescence microscopy by standing-wave excitation", Nature, 1993, 1993366 (6450): 44–8.

[13] Gustafsson MG, "Surpassing the lateral resolution limit by a factor of two using structured illumination microscopy". J Microsc., 2000, 198 (Pt 2): 82–7.

[14] a) Gustafsson MG, "Nonlinear structured-illumination microscopy: Wide-field fluorescence imaging with theoretically unlimited resolution", Proc. Natl. Acad. Sci. U.S.A., 2005, 102 (37): 13081–6; b) **Catherine G. Galbraith, James A. Galbraith, "Super-resolution microscopy at a glance", J Cell Sci. 2011 May 15; 124(10): 1607–1611**

[15] Terukazu Kosako, Yutaka Kadoya, Holger F. Hofmann, Directional control of light by a nano-optical Yagi–Uda antenna, Nature Photonics 4, 312 - 315 (2010).

[16] Shalit, A., Lucchetta, D.E., Piazza, V., Simoni, F., Bizzarri, R, Castagna, R., Polarization-dependent laser-light structured directionality with polymer composite materials, 2012, 81, 232-234;

[17] Shalit, A., Lucchetta, D.E., Criante, L., Vita, F., Tasseva, J.R., Simoni, F., Franco, L., Bizzarri, R., Faraci, P., Conte, R., Viti, L., Kaner, R., Castagna, R., Laser light polarization plastic visualizer: Light scattering distribution and anisotropy, RSC Advances, 2013, 3, 21, 7677-7680.

[18] Lingling Huang, Xianzhong Chen, Holger Mühlenbernd, Guixin Li, Benfeng Bai, Qiaofeng Tan, Guofan Jin, Thomas Zentgraf, Shuang Zhang, Dispersionless Phase Discontinuities for Controlling Light Propagation, Nano Lett. 2012, 12, 5750−5755.

[19] H.P. Nolting, M. Gravert, W. V. Reden, Y-branch - the key component for crosstalk reduced optical switches: modelling analysis, Optical and Quantum Electronics, February 1997, Volume 29, Issue 2, 275–284.

[20] Katsumi Morishita, Wavelength-selective optical-fiber directional couplers using dispersive materials, Optics Letters, 1998, 13(2), 158, 1988.

[21] Pierce J. R., "Coupling of modes of propagations", Journal of Applied Physics, 25, 179 (1954).

[22] Di Donato A., Farina M., Mencarelli D., Lucesoli A., Fabiani S., Rozzi T., Di Gregorio G. M., Angeloni G., "Stationary Mode Distribution and Sidewall Roughness Effects in Overmoded Optical Waveguides", Journal of Lightwave Technology, 2010, 28, 1510-1520.

[23] D.L. Lee, electromagnetic Principles of integrated optics, New York, Wiley, 1986

Acknowledgements

The authors thank Mister Andrea Lucchetta for helping in angular measurements; Prof. Francesco Simoni, from Università Politecnica delle Marche (Ancona, Italy) for the useful and impressive support in discussion and theory construction; Jordanka Tasseva from Italian national institute of nuclear physics, for the equally useful, impressive and constant scientific support, being an expert in Applied Materials fields. On the other hand, she has helped in theory elaboration and scientific discussion, and in revising the manuscript; Dr. Luca Nucara, from Deltatech, s.p.a, Lucca (Italy) for helping in multiplexing measurements; Dr. Melania Paturzo from Istituto di Scienze Applicate e Sistemi Intelligenti, CNR, ISASI-CNR, Pozzuoli, Italy, for the fruitful scientific discussions; Dr. Vito Pagliarulo for helping in profilometric measurements. R. C. strongly thanks Prof. Stefano Luin from NEST, Scuola Normale Superiore di Pisa, since he has given total freedom in using his lasers.

R. C. acknowledges the indispensable financial support of Amedeo Castagna and Maria Teresa Mircoli Castagna.

Dedicated to Alfredo Castagna in occasion of his 2 years (16 March 2020).

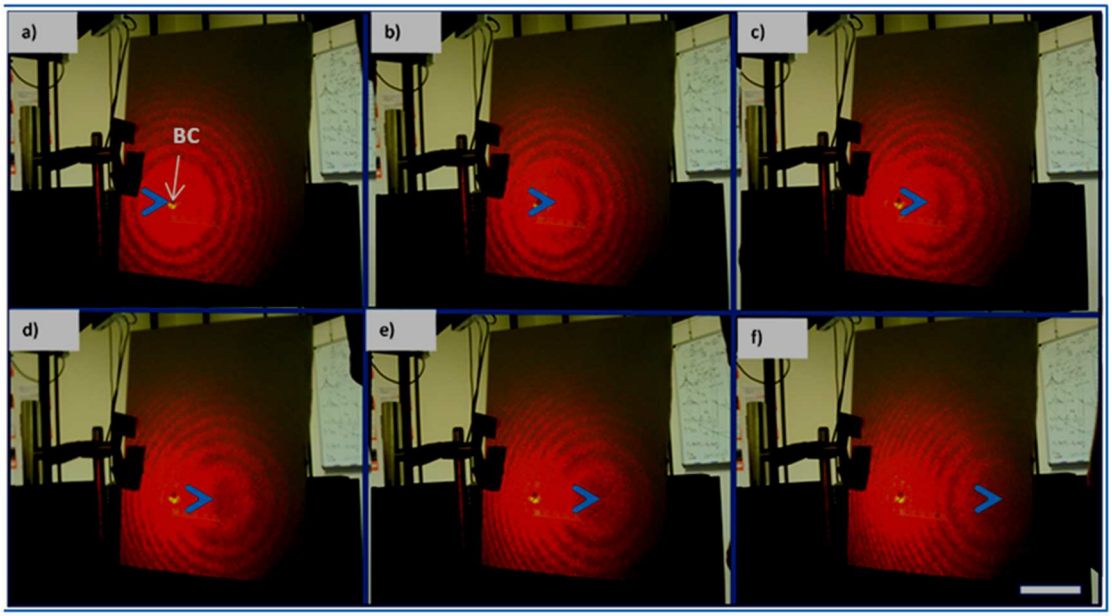

Figure 1. Optical far field pattern obtained when rotating the sample around an axis perpendicular to the optical table: (a) 0.0°; (b) 0.5°; (c) 1.5°; (d) 2°; (e) 2.5°; f) 3°. λ_w = 457.9 nm; λ_r = 632.8 nm. Bar = 5 cm. The blue arrow indicates the center of the concentric rings pattern and allows reading the shift from BC that is the center of the laser beam.

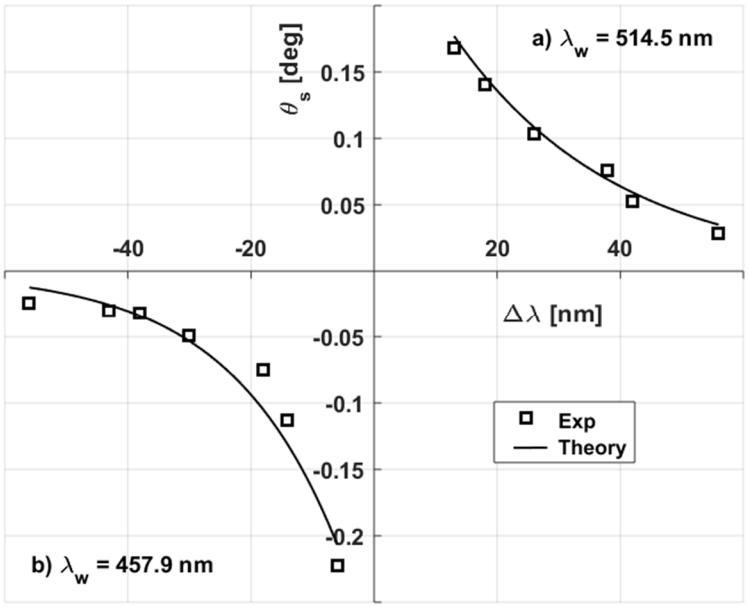

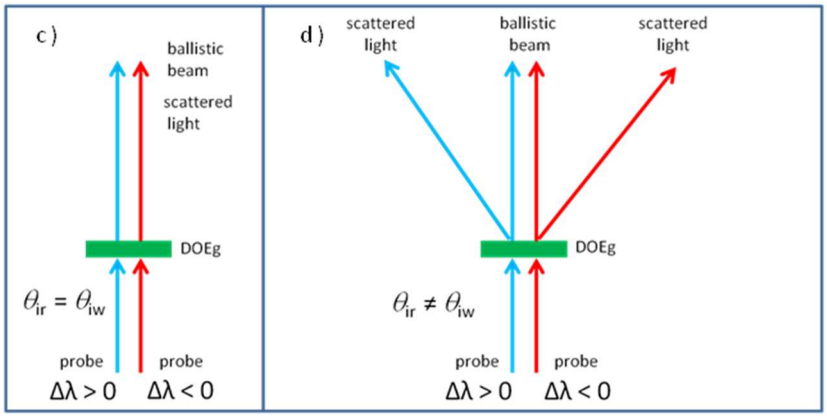

Figure 2. Graph: angular distribution of the scattered light (θs) vs $\Delta\lambda$ (squares = experimental; black line = theory). Angle of incidence of the probes (θ_{ir}) = 0.18°. (a) Writing wavelength λ_w = 514.5 nm; λ_r = 501.5 nm ($\Delta\lambda$ = 13 nm), 496.5 nm ($\Delta\lambda$ = 18 nm), 488 nm ($\Delta\lambda$ = 26.5 nm), 476.5 nm ($\Delta\lambda$ = 38 nm), 472.5 nm ($\Delta\lambda$ = 42 nm) 457.9 nm ($\Delta\lambda$ = 56.6 nm) (b) Writing wavelength λ_w = 457.9 nm; λ_r = 472.5 nm ($\Delta\lambda$ = -14.6 nm), 476.5 nm ($\Delta\lambda$ = - 18.6 nm), 488 nm ($\Delta\lambda$ = - 30.1 nm), 496.5 nm ($\Delta\lambda$ = - 38.6 nm), 501.5 nm ($\Delta\lambda$ = - 43.6 nm), 514.5 nm ($\Delta\lambda$ = - 56.6 nm). The used energy doses are reported in the Materials and Methods Section. Scheme: simplified sketch of the anomalous angular light scattering distribution: DOE (diffractive optical element) written by green light impinging, in this case, perpendicular to the sample. θ_{ir} = angle of incidence of the reading beam; θ_{iw} = angle of incidence of the writing beam; θ_{iw} is chosen perpendicular to the sample just for a better comprehension of the phenomenon; the light-probes used are blue ($\Delta\lambda > 0$) or red ($\Delta\lambda < 0$): c) the probes have the same incidence angle of the writing one ($\theta_{ir} = \theta_{iw}$); the scattered light maintains the ballistic beam direction; d) by keeping $\theta_{ir} \neq \theta_{iw}$, one gets light scattered in two directions, the scattering angle being $\pm\theta$ for $\Delta\lambda > 0$ and $\Delta\lambda < 0$, respectively.

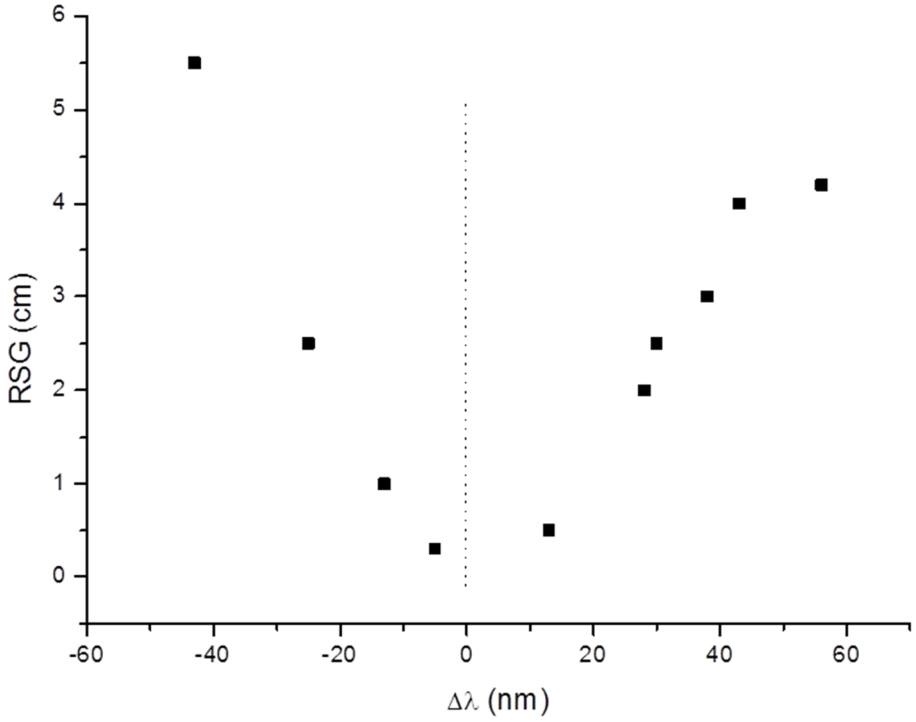

Figure 3. Distance between the sample and the plane where rings start to be differentiated (Rings-Sample Gap, RSG) vs Δλ. RSG is assumed as an indirect evaluation of the focal length.))

SUPPORTING INFORMATION

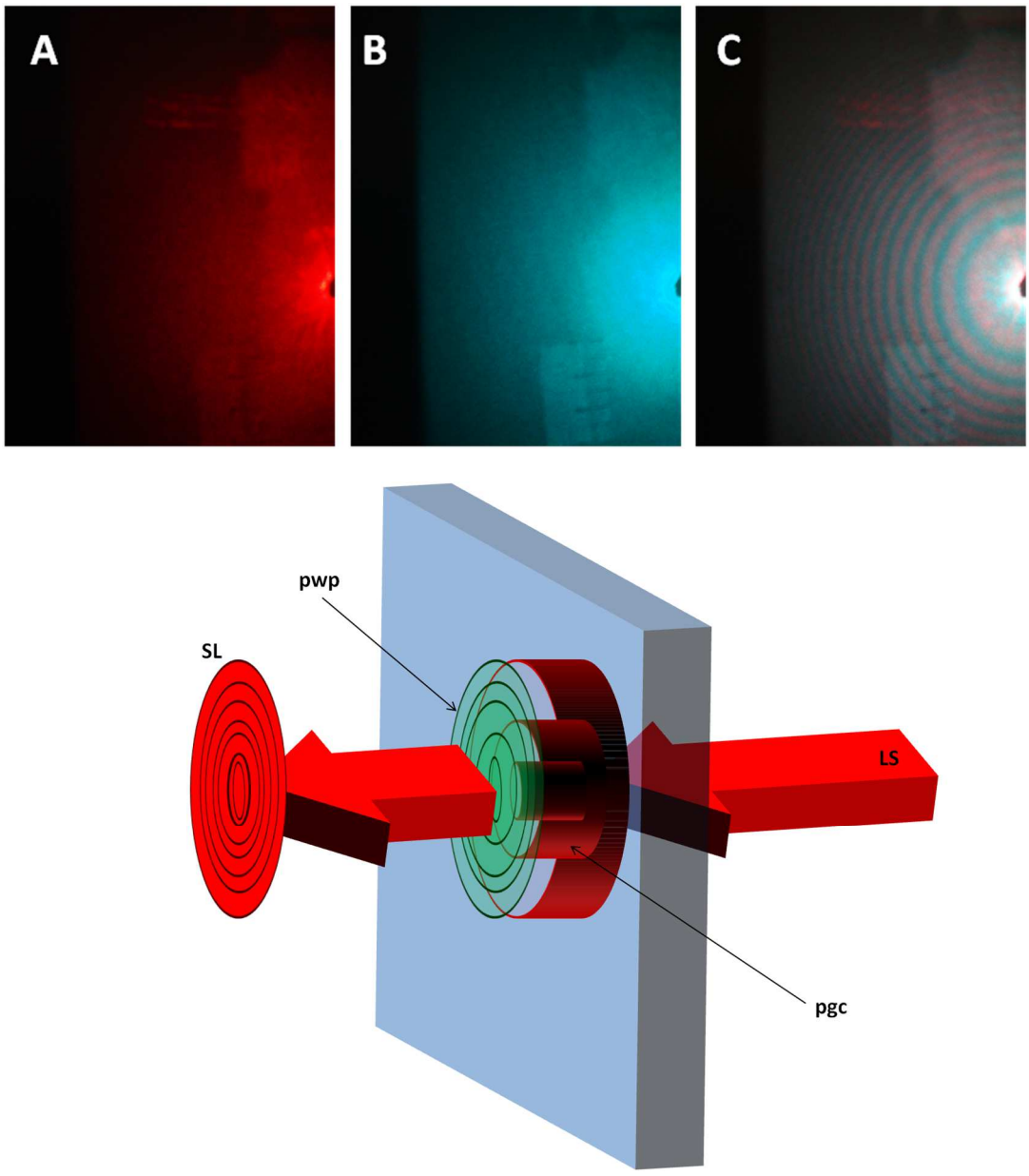

Figure S1.1 A) Far field optical diffraction obtained by using λ_r = 632.8 nm as probe, before polymerization; **B)** under exposure with λ_w = 501.5 nm (polymerizing beam); **C)** optical far field pattern obtained by superimposition of λ_r and λ_w. The rings appearance is due to the

probe diffraction as sketched in **D)**, where LS = laser source; SL = scattered light; pwp = pattern written in the polymer matrix; pgc = pattern generated in the resonant cavity.

Movie MS1: Concentric rings formation by using as a probe λ_r = 632.8 nm and as writing wavelength λ_w = 488 nm. At the beginning, by using the probe, the polymerization doesn't start, since the photo-initiator used is not sensitive to red light: concentric rings are not visible. Then, by superimposing the λ_w = 488 nm, concentric rings appear. As it is visible, by switching-off the blue light, the concentric rings are generated only by the red probe light.

Movie MS2: in this case, λ_w = 457.9 nm, while λ_r = 488 nm, namely $\Delta\lambda < 0$. At the beginning of the experiment, the sample is rotated clockwise and, then, anti-clockwise. The rotation angles are indicated step by step in the Movie. See Experimental for more details. As is evident, the concentric rings shift follows the direction of the sample rotation.

Movie MS3: opposite case with respect to that illustrated in MS2, namely $\Delta\lambda > 0$. In this case, λ_r = 457.9 nm, while λ_w = 488 nm. The rotation angles are indicated step by step in the Movie. See Experimental for more details. As in the previous case, at the beginning of the experiment, the sample is rotated clockwise and, then, anti-clockwise. As is evident in this case, the concentric rings shift doesn't follow the direction of the sample rotation but its opposite.

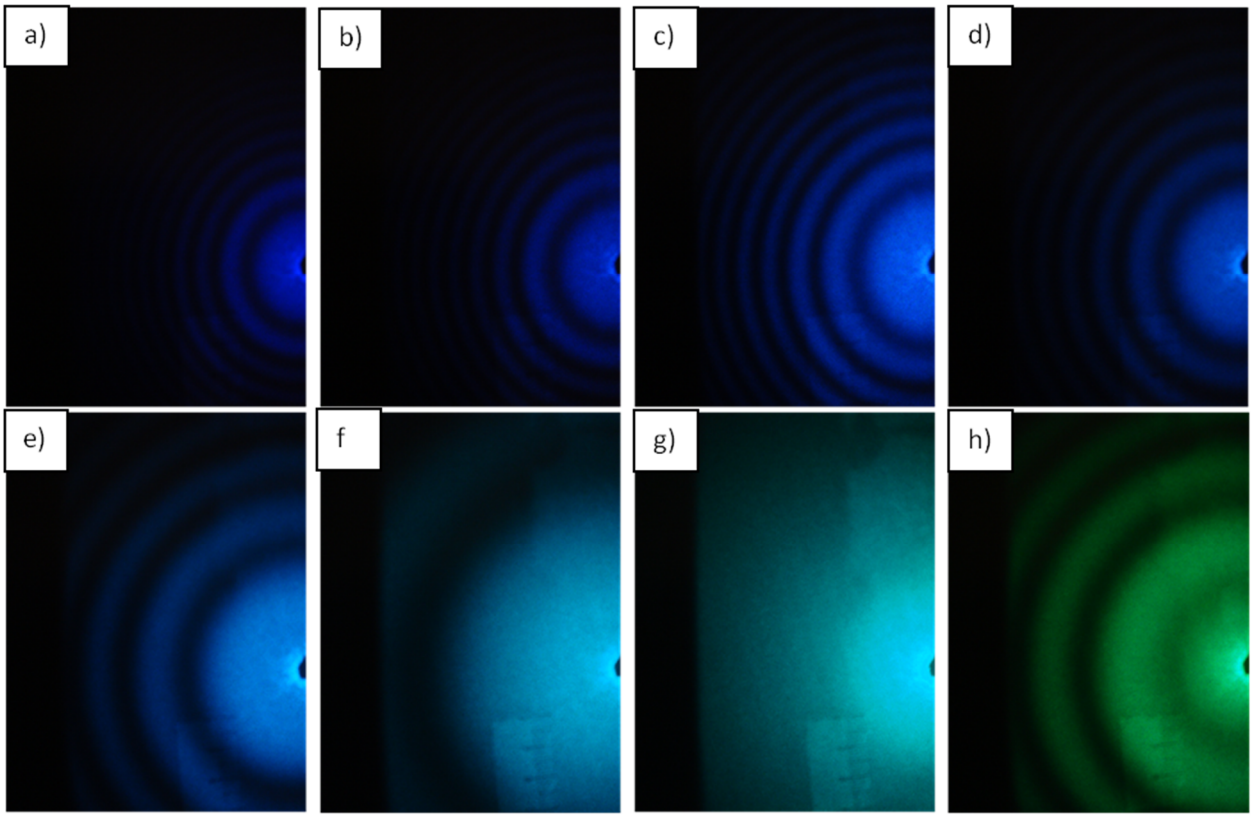

Figure S1.2 Optical far field diffraction patterns obtained with different probes (a) λ_r = 454.5 nm; (b) λ_r = 457.9 nm; (c) λ_r = 472.5 nm; (d) λ_r = 476.5 nm; (e) λ_r = 488 nm; (f) λ_r = 496.5 nm; (h) λ_r = 514.5 nm after writing with (g) λ_w = 501.5 nm.

THEORY FOR MOIRE'-INTERACTIONS BETWEEN STRUCTURED-LIGHT AND MATTER STRUCTURED BY LIGHT:

- THEORY FOR MONODIMENSIONAL GRATINGS IN THIN FILMS

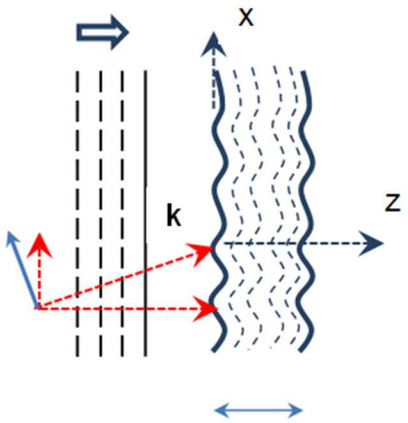

A modulated wave-front, incident on a film with a modulated permittivity, can be decomposed in term of its components in the spatial frequency domain. Each of them, described by an amplitude $a(k_x)$, is a continuous function of the spatial frequency k_x:

$$(1)\quad E(x,z) = e(x)e^{-jk_z z} \xrightarrow{\text{Fourier Transform}} a(k_x)e^{-j\mathbf{k}\cdot\mathbf{r}} = a(k_x)e^{-jk_x x}\, e^{-jk_z z} \qquad e(x) \in C$$

with E some Cartesian coordinate of the vector field and k_z the propagation constant along the propagation direction **z**. The diffraction phenomena can be described by means of Coupled Mode Theory (CMT), by considering the interaction between each spatial component and the continuum spectrum of diffracted waves. For the sake of simplicity, we neglect the back-reflected waves, whereas we assume a film having a finite thickness with a modulated permittivity in the normal plane x-y with a dimension >> period of spatial modulation. In this framework, instead of considering plane wave coupling along the propagation direction z, we change the point of view by rewriting the coupled equations along the x-direction. According to that, each component $a(k_x)$ is now modulated along the direction perpendicular to the wave propagation **z**. The presence of a spatial dielectric perturbation

induces a coupling in the spatial frequency domain between each component of the modulated wave-front. For two wave-planes, with spatial frequencies described by the wavenumbers **k** = (k_x, k_z) and **η** = (η_x, η_z), the amount of power exchanged between them along the x-direction per unit of length, is described by the following coupling coefficient at the temporal frequency $\omega = 2\pi f$ [20, 21]:

(2) $$c(\eta_x, k_x, x) = \frac{\omega}{2} sign(k_x) \iint_S \Delta\varepsilon(x,z)\,\tilde{e}(\eta_z)\,\tilde{e}^*(k_z)\,dS$$

The fields $e(k_z)$ and $e(\eta_z)$ represent two generic plane-waves forming the basis expansion of the incoming wave-front incident on the dielectric perturbation and can be described as:

(3) $$e(k_x) = A_n(k_x)e^{-jk_z z} \qquad A_n(k_x) = \frac{1}{\sqrt{\left\langle |a(k_x)|^2 \right\rangle_{k_x}}}$$

The coefficients A_n have been introduced in order to set the power of incident wave-front to unit, whereas the term $\langle\ \rangle_{kx}$ denotes integration over spatial frequencies. Differently, the expression $\Delta\varepsilon(x,z) = \Delta\varepsilon(x)\cdot\Delta\varepsilon(z) = \Delta\varepsilon f(x)g(z)$ reported in (2), represents the permittivity perturbation in which the z-dependence is due to the finite dimension of film. The term *sign* in (2) denotes the sign function whereas the surface integration is performed over the dielectric perturbation area. According to that analysis, the effect of finite thickness of dielectric film along the z-direction acts only on the coupling coefficient $c(k_x,\eta_x,x)$. Because of the presence of a continuous spectrum of diffracted waves the spatial interaction between the component $a(k_x)$ and diffracted spectrum is described by an integral operator extended over the whole spectrum of scattered spatial frequencies η_x [21]:

(4) $$\frac{d}{dx}a(k_x,x) = -j\int_{-\infty}^{\infty} a(\eta_x,x)\,c(\eta_x,k_x,x)\,e^{j(k_x-\eta_x)x}\,d\eta_x$$

In the eq. (4) each plane wave a(k_x) interacts with the waves propagating in the positive and negative semi-space (+/- *kx*), according to the reference system introduced in the Figure reported above. We have also assumed that no coupling occurs between plane waves and guided modes inside the dielectric film. The above differential equation can be rewritten in term of an integral equation (< >$_x$) whose integration limits can be extended to infinity, as the transverse perturbation has a dimension >> period of spatial modulation. This condition has a strong implication in term of diffracted field, as it describes implicitly a stationary behavior of diffracted field along the x direction, according to the hypothesis assumed:

$$a(k_x,x) = a_0(k_x) - j\int_{-\infty}^{\infty} \left\langle a(\eta_x,x)\, c(\eta_x,k_x,x)\, e^{j(k_x-\eta_x)x} \right\rangle_x d\eta_x \tag{5}$$

The integral equation can be solved iteratively, leading for the n-th order solution to the following equation:

$$a_n(k_x,x) = a_0(k_x) - j\int_{-\infty}^{\infty} a_{n-1}(\eta_x)\,\tilde{C}(\eta_x,k_x,k_x-\eta_x)\, d\eta_x \tag{6}$$

in which $\tilde{C}(k_x) = \Im ourier\{c(x)\}$. The formal expression for the coupling coefficient appears to be equal to:

$$c(k_x,\eta_x,x) = \frac{\omega}{2} sign(k_x)\Delta\varepsilon \cdot f(x)\left\langle g(z)\cdot \tilde{e}(\eta_x)\,\tilde{e}^{*}(k_x)\right\rangle_S \tag{7}$$

The function g(z) describes the finite thickness of film, but could be generalized as shown in the following. From eq. (7) we derive the function:

$$\tilde{C}(k_x,\eta_x,k_z,\eta_z) = \frac{\omega}{2} sign(k_x)\Delta\varepsilon \cdot A(k_x)A(\eta_x)\tilde{F}(k_x-\eta_x)\tilde{G}(k_z-\eta_z) \tag{8}$$

Interestingly, when the film thickness approaches zero, the iterative solution reported in eq. (6) becomes:

(9) $$a_n(k_x,x) = a_0(k_x) - j \cdot a_{n-1}(k_x) * \tilde{C}(k_x)$$

And the final diffracted spectrum can be derived by iterative application of the convolution operator.

Some notes about convolution and its properties. The idea is based on the concept that along the interface direction, if no variation is present, the transverse wavenumber k_x does not change in any way, even in the presence of a dielectric step. Only a transverse perturbation changes the incident spectrum of frequencies k_x (the same reasoning holds for a bi-dimensional wave-front). This leads to a set of coupled equations being defined along the x direction instead of the propagation direction

- THEORY FOR BIDIMENSIONAL GRATINGS IN THIN FILMS

In the case of a 2D dielectric perturbation and bi-dimensional modulated incident wave-front, the above model and set of equations can be generalized by considering for each plane wave the amplitude $a(k_x, k_y)$, forming the basis of expansion of the incoming wave-front. The previous concepts can be extended to the coupling coefficients $c(k_x, k_y, \eta_x, \eta_y)$, depending on the transverse spatial frequencies k_x, k_y, η_x, η_y related to the wavenumbers k, **η** of two generic coupled wave planes, according to the relation:

(10) $$c(\eta_x,\eta_y,k_x,k_y,x) = \frac{\omega}{2} sign(k_x) \iint_S \Delta\varepsilon(x,y,z)\, \tilde{e}(\eta_y,\eta_z)\, \tilde{e}^*(k_y,k_z)\, dS$$

The spatial interaction between each components $a(k_x,k_y)$ is now described by the integral operator [21]:

(11) $$\frac{d}{dx}a\left(k_x,k_y,x\right)=-j\int_{-\infty}^{\infty}\int_{-\infty}^{\infty}a\left(\eta_x,\eta_y x\right)c\left(\eta_x,\eta_y,k_x,k_y,x\right)e^{j\left(k_x-\eta_x\right)x}d\eta_x d\eta_y$$

with

$$\tilde{e}\left(k_y,k_z\right)=A_n\left(k_x\right)e^{-jk_z z}e^{-jk_y y}$$

The iterative expression becomes:

(12) $$a_n\left(\mathbf{k}_t,x\right)=a_0\left(\mathbf{k}_t\right)-j\int_{-\infty}^{\infty}a_{n-1}\left(\boldsymbol{\eta}_t\right)\tilde{C}\left(\boldsymbol{\eta}_t,\mathbf{k}_t,k_x-\eta_x\right)d\eta_x \quad \mathbf{k}_t=\left(k_x,k_y\right)$$

whereas in the thin film approximation, the following equation holds:

(13) $$a_n\left(\mathbf{k}_t,x\right)=a_0\left(\mathbf{k}_t\right)-j\cdot a_{n-1}\left(\mathbf{k}_t\right)*\tilde{C}\left(\mathbf{k}_t\right)$$

- ELECTRIC FIELD OF THE LIGHT INSIDE THE GLASS DURING READING AND SPATIAL DISTRIBUTION OF THE REFRACTIVE INDEX

The spatial distribution of the refractive index of the written polymer and the electric field of the light inside the glass during reading can be deduced according the following considerations. During the recording process, the organic layer generates conical scattered light that interferes with the backscattering light generated inside the same layer, due to the partially reflections by the glass entrance surface. As a consequence interference between quasi-spherical waves is generated and a concentric ring light pattern is recorded in the polymer leading to a ring modulated refractive index. After the photo-polymerization, the interference conditions are still fulfilled for the probe beam, which is now scattered by the polymerized region. According to this assumption, an interaction occurs between (ring-

shaped) structured light and (ring-shaped) structured film, which gives rise to the observed transmitted pattern. It's important to highlight that the relevant aspect is not the specific geometry leading to light interference but the concept of scattering between a modulated wave and an index modulated film. In this framework we start by considering the phase difference $\Delta\varphi = \varphi_1 - \varphi_2 = k(s_1 - s_2)$ between two interfering spherical waves, with $k = 2\pi/\lambda$:

(14) $$E_1(r,z) = \frac{A_1}{s_1} e^{j\varphi_1} \qquad E_2(r,z) = \frac{A_2}{s_2} e^{j\varphi_2}$$

having assumed for the sake of simplicity the same polarization. According to Eq. (14), the intensity distribution in a generic point *P(r,z)* inside the polymeric film is given by the following relation:

(15) $$I(r,z) = \frac{A_1^2}{s_1^2} + \frac{A_2^2}{s_2^2} + 2\frac{A_1 A_2}{s_1 s_2}\cos\Delta\varphi$$

As a consequence, the interference pattern gives rise to a polymer permittivity modulation equal to:

(16) $$\varepsilon(r,z) = \varepsilon_0 + \Delta\varepsilon(r,z) = C\left[\frac{A_1^2}{s_1^2} + \frac{A_2^2}{s_2^2} + 2\frac{A_1 A_2}{s_1 s_2}\cos\Delta\varphi\right]$$

where C is a dimensional constant parameter.

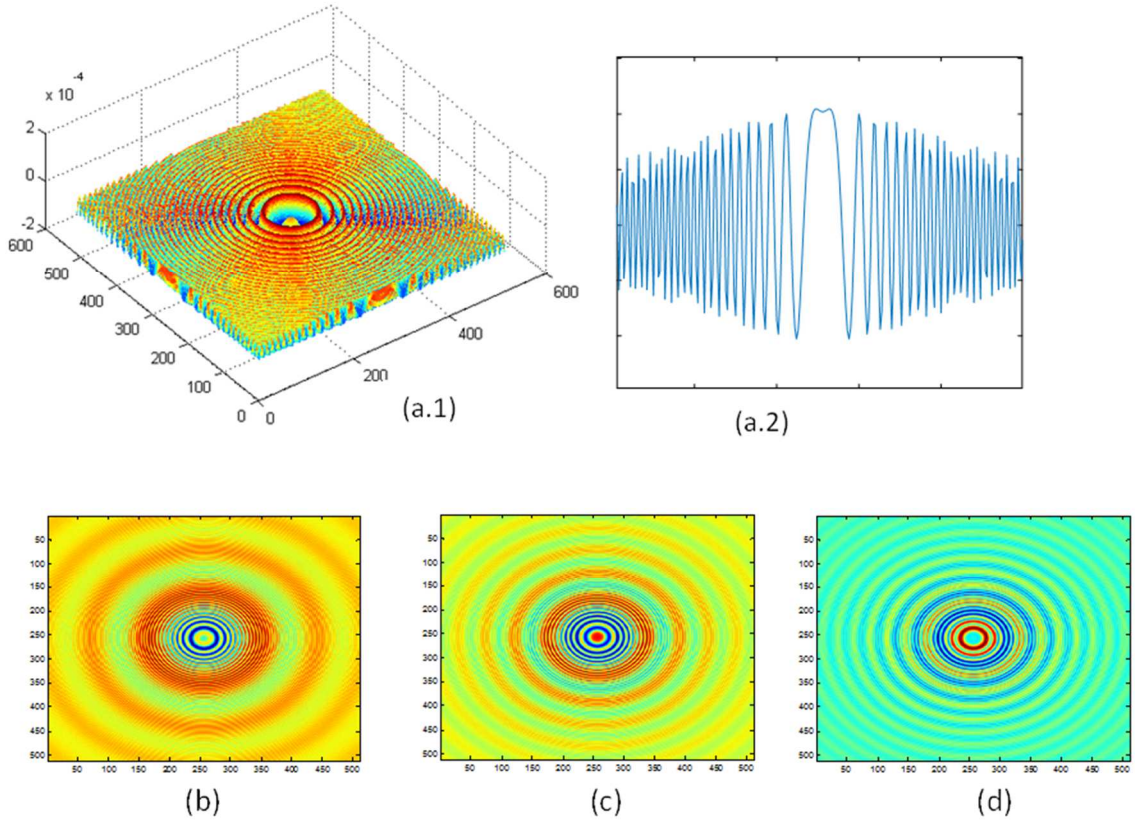

Graph S1 Simulated patterns for : a) refractive index distribution in the polymer film (a.1.: 2D distribution; a.2. profile of refractive index distribution); b), c), d) optical far field patterns obtained at $\Delta\lambda$ = 50nm, $\Delta\lambda$ = 100 nm and $\Delta\lambda$ = 200 nm, respectively.

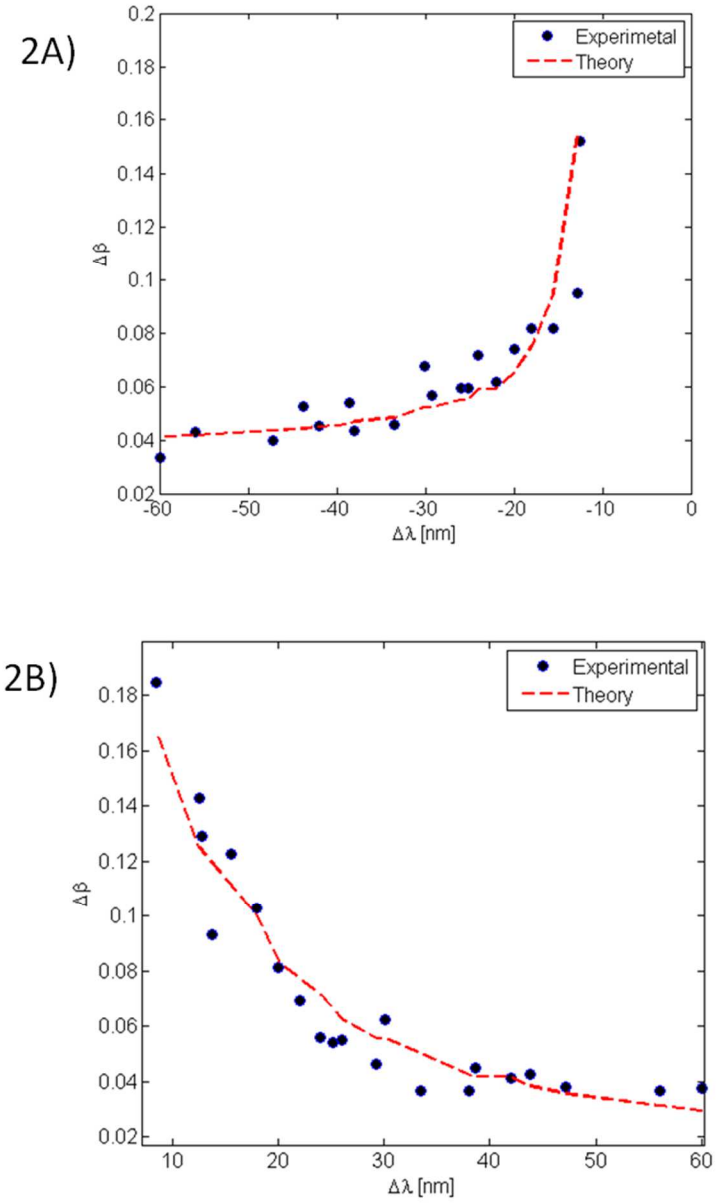

Figure S2 Dependence of the angular distribution of the ring pattern small angle ($\Delta\beta$) on $\Delta\lambda$. $\Delta\beta$ is determined by the distance (in cm) between the n^{th} ring and the $(n-1)^{th}$ ring, normalized to the minimum distance between the sample and the screen. The curve in **S2A)** relates to $\Delta\beta$ vs $\Delta\lambda < 0$, while the curve in S**2B)** relates to $\Delta\beta$ *vs* $\Delta\lambda > 0$. The dashed red lines are the theoretical curves. With the available laser source the rings are observed at a minimum distance $\Delta\lambda$ = 8.5 nm, in our experimental conditions. Thus, the achievable wavelength resolution should be lower than this value.

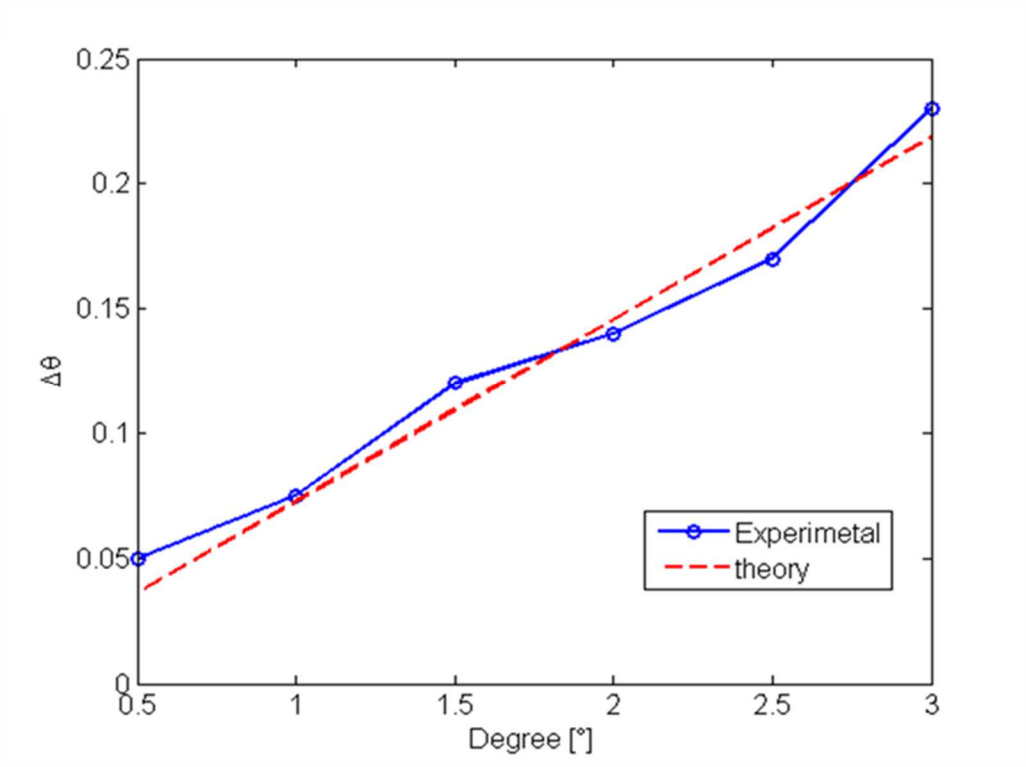

Figure S4 Angular shift ($\Delta\theta$) vs sample's rotation (deg°) when the sample is distant 42.5 cm from the screen where the optical far field pattern is collected (λ_w= 457.9 nm; λ_r = 632.8 nm).

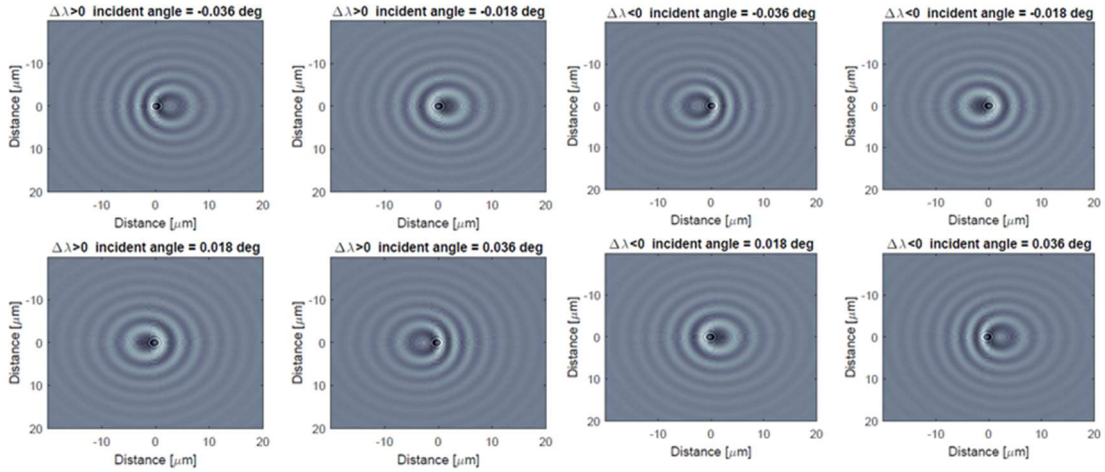

Figure S5 Numerical Analysis regarding the shift of the rings pattern vs Δλ at four different incidence angles for the laser probe (λ_r) and considering the glass thickness = 1 mm.

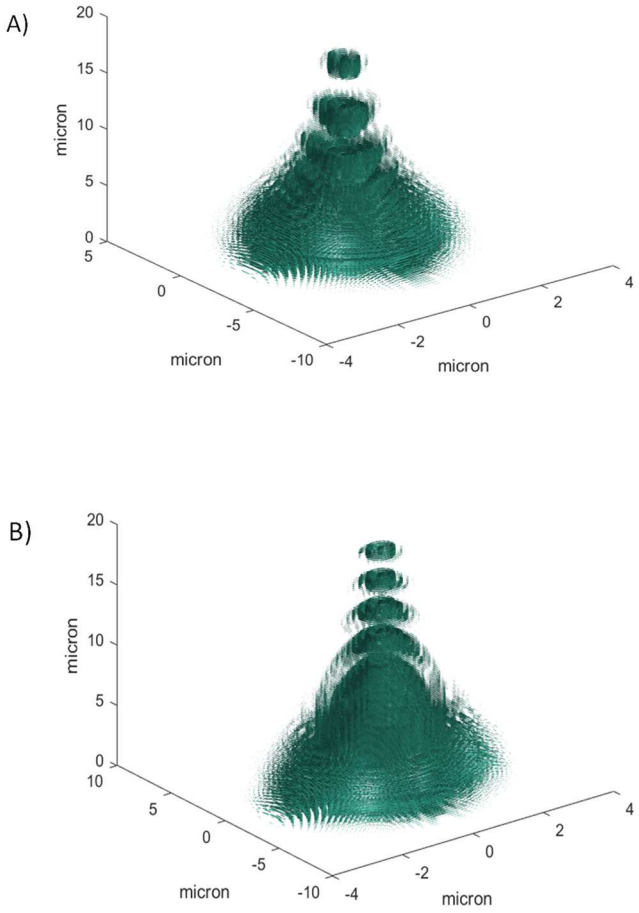

Figure S6 Numerical Simulation of a pattern of light generated at $\Delta\lambda > 0$ (S5.A) and $\Delta\lambda < 0$ (S5.B) into the material. It is evident that the light in the system tends to converge with higher speed for $\Delta\lambda > 0$ than for $\Delta\lambda < 0$.

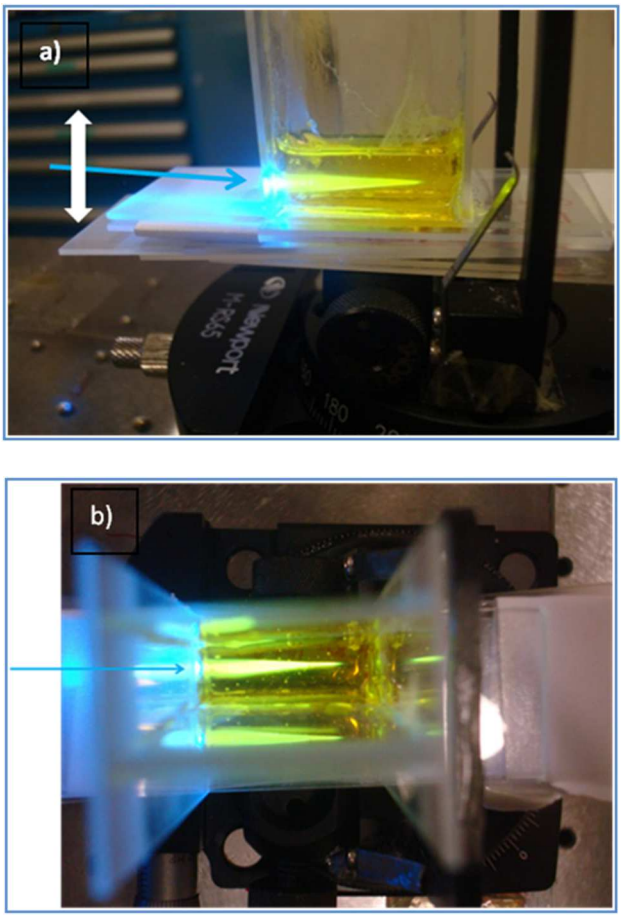

Figure S7 An image of irradiation of the photopolymerizable mixture. In this case, the mixture is placed in a glass cuvette of c.a. 1 cm x 0.5 cm. The volume of the mixture is c.a. 1.0 cm x 0.5 cm x 0.5 cm. a) The polymerizing laser single beam from the left side of the picture (blue arrow) enters in the lateral narrower side of the cuvette (λ = 476.5 nm; power P = 78 mW). Note that at the edge of the cuvette a polarization-dependent effect is visible (blue light at the border of the first glass): the light is scattered perpendicularly to the polarization vector of the beam. b) View from above: the impinging light is indicated with the blue arrow.

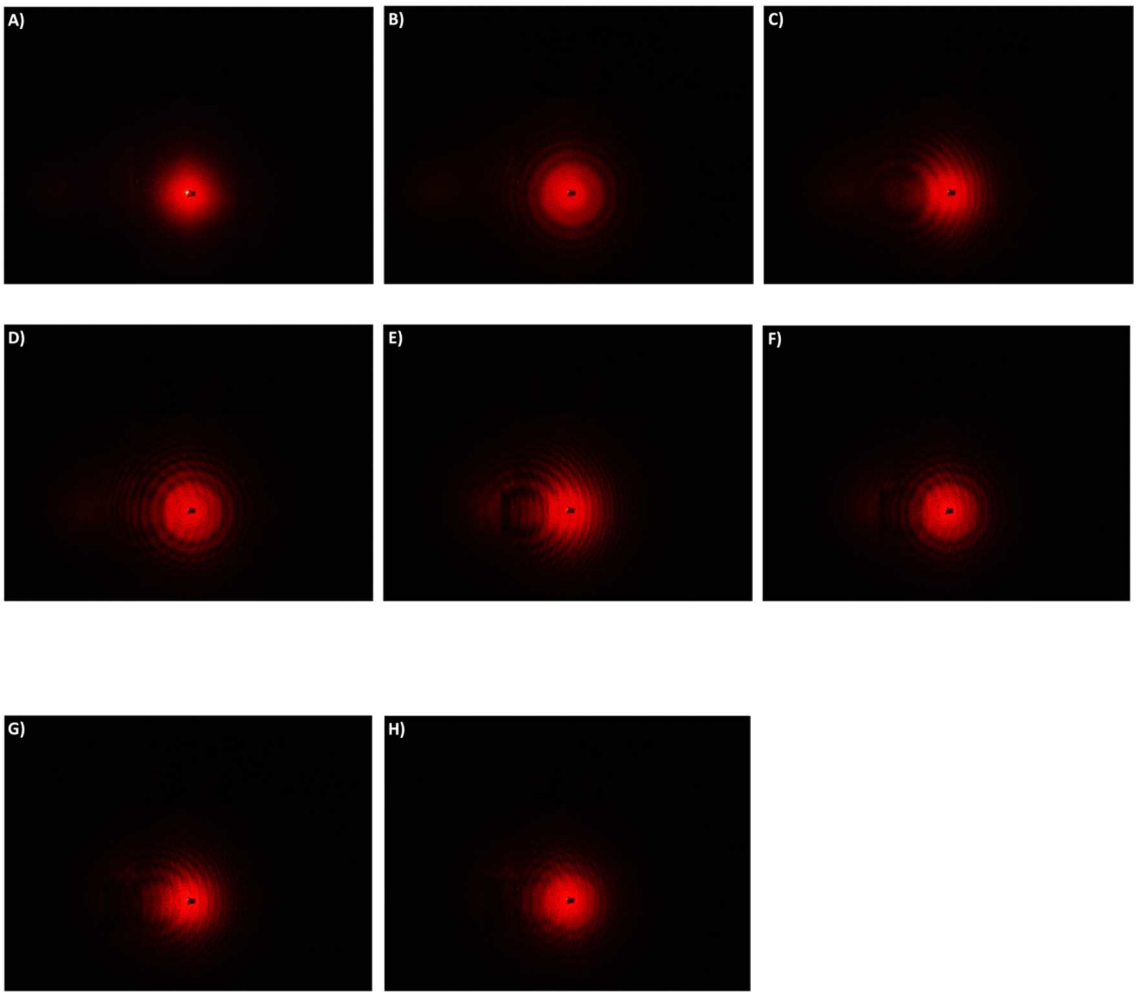

Figure S8 Multiplexing information by the superimposition of patterns obtained at different wavelengths and angles. Probe at λ_r = 632.8 nm; λ_w at 514.5 nm (b); 496.5 nm (d); 488 nm (f); 476.5 nm (h). a) before writing (unpolymerized material); b) λ_w = 514.5 nm; c) the sample is rotated 1°; d) on the same sample written again at λ_w = 496.5 nm; e) the sample is rotated of 1° more; f) on the same sample written again at λ_w = 488 nm; g) the sample is rotated of 1° more (three degrees from the beginning of the process); h) on the same sample written again at λ_w = 476.5 nm.

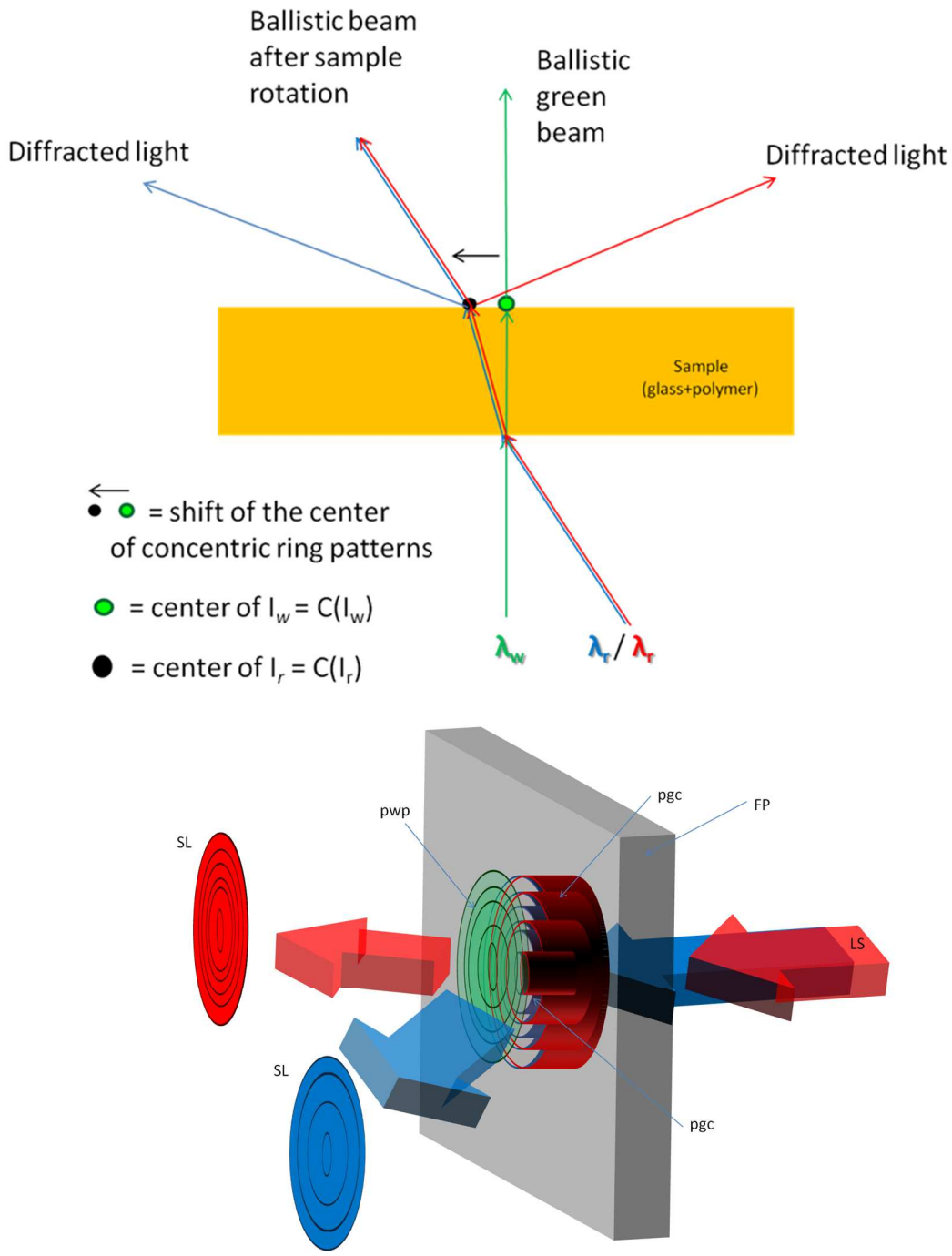

Scheme S9 a) (up) When rotating the sample, the incoming diffracted light has a center slightly shifted from the center of the recorded refractive index distribution. The numerical simulations are reported in Figure S1 and are plotted in Figure 2 (theory line). A further sketch is reported in **b) (down)**: LS = laser source; SL: scattered light; pwp = pattern written in the polymer; pgc = pattern generated in the cavity.

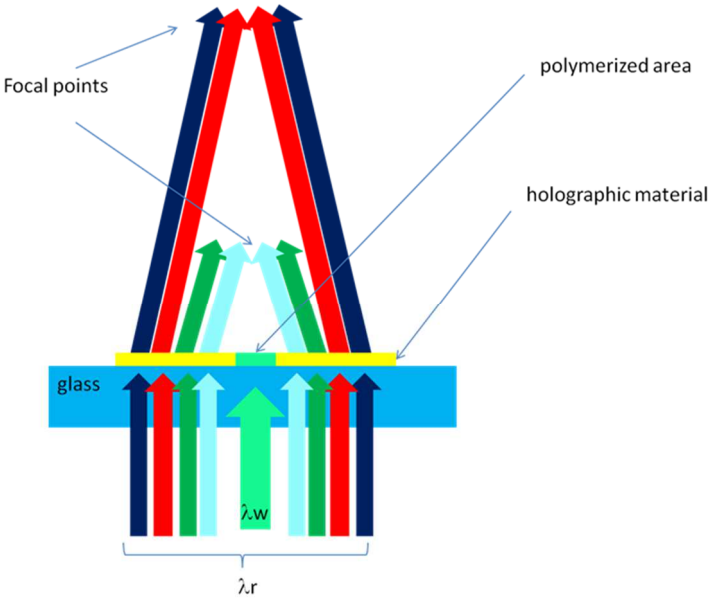

Scheme S10 Sketch of the achromatic system presenting two different λ_r focusing on the same focal point, for each focal point.